Amphiphilic Inorganic Nanoparticles with Mixed Polymer Brush Layers of Variable Composition: Bridging the Paradigms of Block Copolymer and Nanoparticle Self-Assembly

Brian R. Coleman & Matthew G. Moffitt

March 2018

Amphiphilic Inorganic Nanoparticles with Mixed Polymer Brush Layers of Variable Composition: Bridging the Paradigms of Block Copolymer and Nanoparticle Self-Assembly

Brian R. Coleman and Matthew G. Moffitt*

Department of Chemistry, University of Victoria, P.O. Box 3065, Victoria, BC, Canada V8W 3V6

Abstract

The application of molecular self-assembly principles to nanoscopic building blocks can inform new pathways to hierarchical nanomaterials. For instance, amphiphilic brush nanoparticles (ABNPs) are inorganic nanoparticles functionalized with mixed polymer brushes of hydrophobic and hydrophilic chains which possess several structural and chemical features similar to amphiphilic block copolymers (ABCs), including spatial segregation of covalently connected hydrophilic and hydrophobic regions, anisotropic interactions, and conformational flexibility. However, the phase behaviour of ABNPs with respect to hydrophobic fraction, concentration, and salt content has not been established to date, precluding direct comparison with ABC self-assembly. In this study, we produce and characterize a series of ABNPs with similar cadmium sulfide (CdS) core sizes and brush densities but with different polystyrene/poly(methacrylic acid) (PS/PMAA) brush compositions using a diblock copolymer mixed micelle approach. Self-assembly of the resulting ABNPs in THF/water mixtures yields hybrid spheres, cylinders, and vesicles with morphological transitions following similar trends with respect to hydrophobic fraction, initial concentration, and salt content to those previously established for ABCs. The resulting ABNP phase behaviour demonstrates that microphase separation principles established in the 1990s for the solution self-assembly of macromolecular ABCs can provide vital experimental guidelines for the controlled self-organization of nanoscopic amphiphiles.

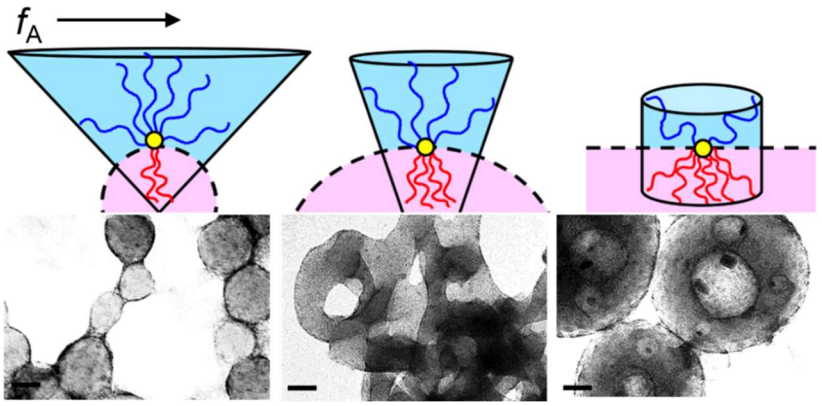

Introduction

As observed by Whitesides over 15 years ago, the general features of molecular recognition can be usefully applied to the controlled self-organization of objects much larger than molecules.[1] For example, a key challenge for future applications of inorganic nanoparticles, including quantum dots and gold nanoparticles,[2-5] is their spatial organization into hierarchical assemblies of controlled size and shape.[6-10] Inspired by the complexity and diversity of spontaneous structure formation from molecular amphiphiles such as surfactants, phospholipids and block copolymers, several groups have focussed on developing inorganic nanoparticles with surface chemistry designed to promote tunable self-assembly of nanoscale building blocks.[6, 7, 11, 12] For example, amphiphilic brush nanoparticles (ABNPs) are inorganic nanoparticles functionalized with mixed polymer brushes containing both hydrophilic and hydrophobic chains.[13-28] These chemically dissimilar polymer chains are either specifically patterned at the inorganic nanoparticle surface[16, 20] or else undergo localized segregation in selective solvents,[21-25] triggering anisotropic interactions between ABNPs and self-assembly into a variety of multiscale superstructures. Although intriguing theoretical results have outlined design principles for controlled self-assembly of idealized nanoscale amphiphiles,[12, 29-32] experimental insights into the phase behaviour of nanoparticle self-assembly, especially those informed by appropriate molecular analogues, are still extremely rare.

Although molecular and nanoscopic amphiphiles exhibit distinct self-assembly behaviour due to differences in scale, geometry and chemical composition,[26] qualitative but systematic similarities between the self-organization of amphiphilic objects on different length scales could provide important conceptual bridges between established molecular principles and new nanomaterials. It has often been noted that ABNPs resemble nanoscale versions of amphiphilic

block copolymers (ABCs) in several respects.[6, 7, 13, 14, 16] The investigation and understanding of the self-assembly behaviour of ABCs was pioneered by Eisenberg and co-workers in the 1990s,[33, 34] who showed that ABC self-assembly could form multiple morphologies that were easily tunable by varying the copolymer composition[35, 36] or chemical environment (e.g. solvent,[37] polymer concentration,[38, 39] and acid/salt additives[40, 41]). ABC morphological transitions were explained by the interplay of three free energy terms: 1.) interfacial tension, 2.) hydrophobic block stretching, and 3.) hydrophilic block repulsion.[33, 34, 36] ABNPs possess several structural and chemical features similar to molecular characteristics of ABCs, including spatial segregation of covalently connected hydrophilic and hydrophobic regions, anisotropic interactions, and conformational flexibility.[23] However, a set of thermodynamic guidelines for controlling morphologies and dimensions of ABNP assemblies, analogous to microphase separation principles established for ABCs,[33, 34, 36] has been missing from the literature. A possible impediment to bridging the self-assembly behaviour of these size-disparate building blocks is the relative synthetic challenge of producing well-characterized ABNPs of variable composition and constant size compared to established polymerization routes to ABCs of variable composition and constant mean molecular weight.[33, 34]

A previous study from our group produced ABNPs consisting of inorganic cadmium sulfide nanoparticles decorated with brush layers containing equal numbers of hydrophobic polystyrene (PS) and hydrophilic, ionizable poly(methacrylic acid) (PMAA) chains.[23] We used the triblock copolymer polystyrene-*block*-poly(acrylic acid)-*block*-poly(methyl methacrylate) (PS-*b*-PAA-*b*-PMMA) to form inverse micelles which were then used as templates to grow individual CdS nanoparticles in each micelle core,[42, 43] followed by hydrolysis of PMMA chains to PMAA.[23] We demonstrated self-assembly of the resulting ABNPs in tetrahydrofuran (THF) / water mixtures to generate spherical supermicelles, vesicles, and segmented wormlike aggregates. The ABNPs

exhibited several characteristics of ionic ABCs in aqueous media including ionic strength-dependent self-assembly behaviour.[40, 41] However, the ABNP phase behaviour with respect to a key self-assembly parameter of ABCs, namely amphiphile composition, could not be established in that work since the triblock copolymer template forced the number of PS and PMAA blocks to be the same.

In this study, we produce a unique series of ABNPs of similar size and structure but variable brush composition using a mixed micelle approach. First, inverse mixed micelles containing different relative quantities of constituent PS-*b*-PAA and PMMA-*b*-PAA diblock copolymers are generated, followed by templated CdS growth and crosslinking in the micelle cores to form hydrophobic mixed brush nanoparticles (Scheme 1). Subsequent PMMA hydrolysis to PMAA (Scheme 2) produces ABNPs with mixed brushes containing various relative numbers of hydrophobic and hydrophilic chains. The resulting ABNPs are then used to investigate the effects of amphiphile composition, initial concentration and salt content on self-assembled morphologies in aqueous media. We find consistent similarities between morphological trends with respect to each of these parameters and those reported previously for solution self-assembly of ABCs,[33, 34] indicating the applicability of microphase separation principles to both macromolecular ABCs and nanoscale ABNPs. This scale invariance of self-assembly motifs suggests that the considerable knowledge of solution self-assembly of ABCs collected over the past 20 years[33, 34] can provide compelling new pathways to nanoparticle-based materials of controlled structure and function.

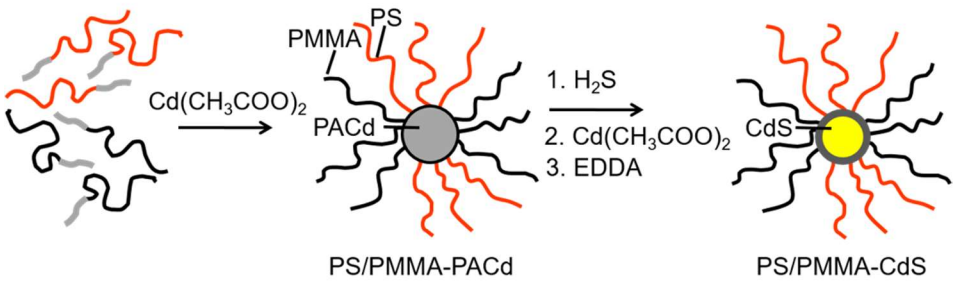

Scheme 1. Formation of PS/PMMA-PACd from diblock copolymer blends and subsequent formation of PS/PMMA-CdS.

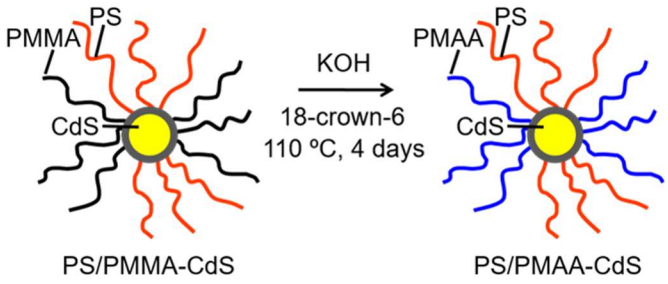

Scheme 2. Hydrolysis of hydrophobic PS/PMMA-CdS to amphiphilic PS/PMAA-CdS.

Results and Discussion

Characterization of Hydrophobic Mixed Brush CdS Nanoparticles (PS/PMMA-CdS).

Our method for producing CdS nanoparticles functionalized with mixed brush layers of PS and PMMA chains of various compositions is described in Scheme 1. The characterization of cadmium acrylate core inverse micelles (PS/PMMA-PACd) prior to CdS growth and crosslinking is described in *Supporting Information.* Based on ^{1}H NMR data, the PS mole fractions for the three PS/PMMA-PACd micelles were determined to be f_{PS} = 0.46, 0.60, and 0.78, representing an approximately even spread of composition values. Since gel permeation chromatography (GPC) results show that mixed micelles maintain structural integrity in subsequent synthesis steps, the

same f_{PS} values (rounded to f_{PS} = 0.5, 0.6, and 0.8 for sample designation) also refer to the PS/PMMA-CdS (Table 1) and PS/PMAA-CdS samples.

All three PS/PMMA-CdS samples yielded clear yellow dispersions in THF, toluene, chloroform and acetone, except the f_{PS} = 0.8 composition in acetone, which was turbid but did not give rise to any observed precipitation (Figure 1). Since acetone is a poor solvent for PS but a good solvent for PMMA, the lack of precipitation in acetone demonstrated a mixed brush structure for all three PS/PMMA-CdS compositions. Comparing GPC traces of PS/PMMA-PACd and PS/PMMA-CdS in THF (Figure S6, *Supporting Information*) showed that templated CdS growth and core crosslinking did not increase the single chain fractions, indicating that the structural integrity of surrounding polymer brushes was retained.

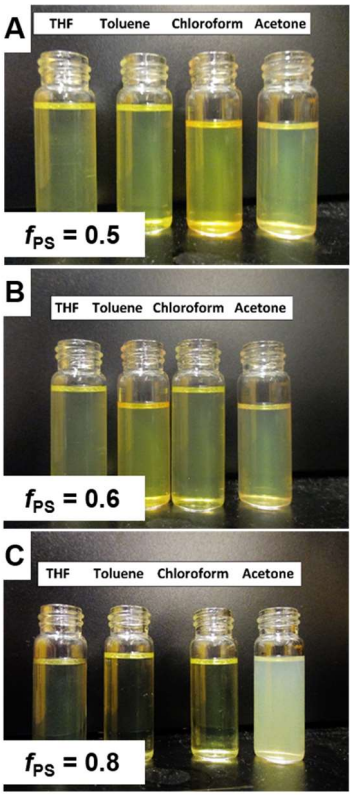

Figure 1. Dispersibility tests for PS/PMMA-CdS samples of variable brush composition in solvents of different polarity: A) f_{PS} = 0.5; B) f_{PS} = 0.6; C) f_{PS} = 0.8.

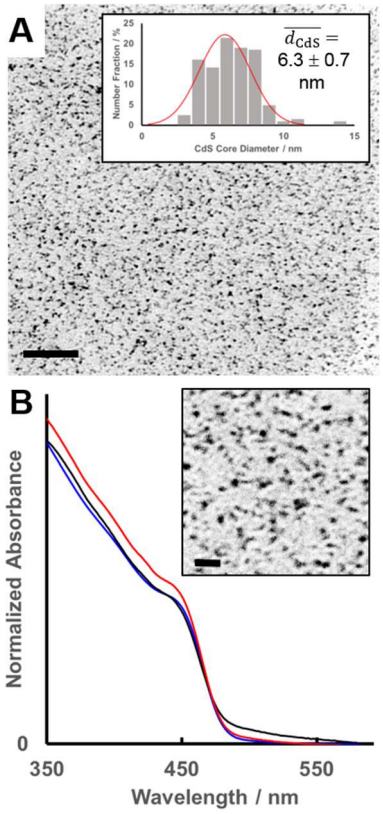

Figure 2. Characterization of CdS cores of PS/PMMA-CdS (f_{PS} = 0.5). A) TEM showing dark CdS cores of benzene-cast PS/PMMA-CdS (scale bar = 100 nm) and associated size distribution (inset); B) UV-Vis of PS/PMMA-CdS dispersed in chloroform (blue), toluene (red), and THF (black) with inset showing high-magnification TEM image of CdS cores (scale bar = 20 nm).

The CdS cores of the three PS/PMMA-CdS samples were characterized by transmission electron microscopy (TEM) and UV-Vis absorbance spectroscopy (Figure 2 and Figure S8, *Supporting Information*). The size distributions of CdS nanoparticle were determined from statistical analysis of TEM images of benzene-cast PS/PMMA-CdS. Average CdS core sizes from TEM size histograms are very similar for the three brush compositions, in the range of d_{CdS} = 6.1-6.3 nm. A high-magnification TEM image is shown in the inset to Figure 2B, revealing the CdS nanoparticles to be roughly spherical in shape. UV-Vis absorbance spectra for the f_{PS} = 0.5 composition in THF, toluene, and chloroform (Figure 2B) show a blue-shifted absorption threshold

(λ_{thresh} = 479 nm) relative to bulk CdS (λ_{thresh} = ~500 nm) and a distinct exciton shoulder (λ_{ex} = 455 nm) indicating quantum confinement. The three spectra in different solvents show strong overlap indicating stability of CdS cores in different media. Similar UV-Vis spectra in all three solvents were obtained from the other two PS/PMMA-CdS samples (Figure S8), further supporting that stable and similar-sized CdS cores (d_{CdS} = ~6 nm) surrounded by mixed polymer brushes of variable composition (f_{PS}) had been produced.

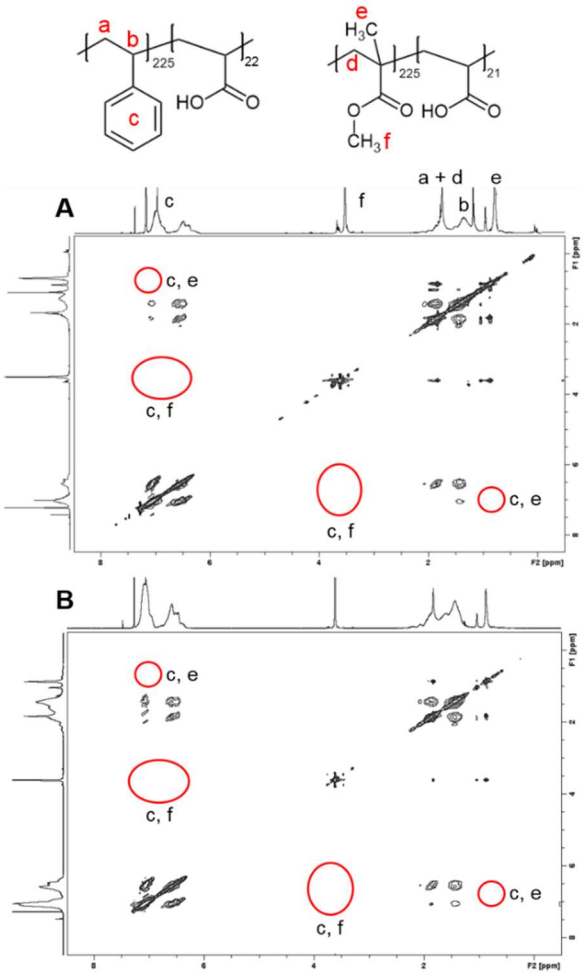

Figure 3. 2D ^{1}H NMR NOESY spectra of (A) PS/PMMA-CdS (f_{PS} = 0.5) and (B) 50/50 blend of PS-*b*-PAA and PMMA-*b*-PAA single chains in chloroform-d. Circles indicate regions of expected cross-peaks between PS and PMMA protons. Similar to the reference of single chains (B), no cross-peaks are observed in PS/PMMA-CdS (A) suggesting chain segregation in the mixed brush.

We applied 2D ^{1}H NOESY experiments to investigate the distribution of PS and PMMA chains within the PS/PMMA-CdS mixed brushes (Figure 3). ^{1}H NOESY probes through-space interactions of proximal protons (< 0.5 nm) and can therefore indicate whether PS and PMMA chains are statistically mixed or compartmentalized within a mixed brush structure. In our previous investigation of PS/PMMA-CdS nanoparticles synthesized from a PS-*b*-PAA-*b*-PMMA triblock copolymer template, ^{1}H NOESY showed distinct symmetric cross-peaks between the phenyl ring protons on PS and both the methyl protons and ester methyl protons on PMMA, indicating proximal interactions which suggested a statistical distribution of PS and PMMA chains.[42] In contrast, all three PS/PMMA-CdS compositions reported here (Figure 3A for f_{PS} = 0.5 and Figure S9 for f_{PS} = 0.6 and 0.8, *Supporting Information*) show an absence of such cross-peaks (red circled regions) similar to the reference of an unmicellized blend of single chains (Figure 3B).

The absence of cross-peaks in 2D ^{1}H NOESY spectra on its own is not sufficient to conclude chain segregation in the of PS/PMMA-CdS brushes, since NOEs can be attenuated by a number of factors characteristic of a specific system (e.g. solvent viscosity, chain molecular weight).[12] However, the absence of cross-peaks in the current mixed brush nanoparticles compared to the presence of cross-peaks in the previous mixed PS/PMMA-CdS brushes of similar chain molecular weights and in solvents of similar viscosity (deuterated THF[42] vs. chloroform-d) provides indirect evidence of the lack of chain mixing in the current case. We therefore infer a "patchy" distribution of PS and PMMA chains in the mixed brush nanoparticles formed from diblock copolymers compared to the random distribution of chains in the mixed brush nanoparticles formed from a triblock copolymer.[42] This difference may be due to a lower entropic penalty of coronal chain segregation when dissimilar PS and PMMA chains are not covalently coupled within the same molecule.

Table 1. Structural Characteristics of PS/PMMA–CdS of Various Brush Compositions Determined from Static and Dynamic Light Scattering in THF

f_{PS}	Z	r_g, nm	σ, chains nm^{-2}	$r_{h,0}$, nm	t_b, nm	*extension*, %	$r_g/r_{h,0}$
0.46	121 ± 10	60 ± 9	0.44 ± 0.04	48 ± 2	43 ± 3	76 ± 5	1.3 ± 0.2
0.60	94 ± 3	39 ± 4	0.39 ± 0.01	22.5 ± 0.5	18.1 ± 0.5	32.2 ± 0.9	1.7 ± 0.1
0.78	113 ± 7	41 ± 7	0.43 ± 0.03	27.0 ± 0.2	22.4 ± 0.5	39.8 ± 0.8	1.5 ± 0.2

The structural characteristics of the three PS/PMMA-CdS samples determined by static and dynamic light scattering (SLS and DLS) in THF are reported in Table 1. Importantly, aggregation numbers based on SLS data for the three brush compositions fall in the range of Z = 94 – 121, all within 15 % of the mean value (Z = 110) and chain surface densities are σ = ~0.4 chains/nm^2 for all three brush compositions. Z values from SLS data are consistent with individually dispersed mixed brush particles. From DLS data, hydrodynamic sizes in THF are consistently larger than the CdS cores due to contributions from the solubilized mixed brushes. Hydrodynamic radii are similar for the f_{PS} = 0.6 and f_{PS} = 0.8 compositions ($r_{h,0}$ = 22 and 27 nm) but about 2 times larger ($r_{h,0}$ = 48 nm) for the f_{PS} = 0.5 mixed brush. A possible explanation for the more expanded brush structure is denser *local* packing of segregated PS and PMMA chains in the f_{PS} = 0.5 case (despite similar *average* brush densities, Table 1) due to more developed phase separation between PS and PMMA chains at the symmetric blend composition. Thus the combination of light scattering results indicates similar brush structures (Z = ~110 and σ = ~0.4 chains/nm^2) in the series of PS/PMMA-CdS of variable brush composition (f_{PS}).

Characterization of Amphiphilic Mixed Brush CdS Nanoparticles (PS/PMAA-CdS). To produce ABNPs from the hydrophobic mixed brush PS/PMMA-CdS samples, the hydrophobic methyl methacrylate repeat units were completely hydrolyzed to hydrophilic methacrylic acid repeat units using KOH catalysis and 18-crown-6 in refluxing dioxane (Scheme 2), as confirmed

by ^{1}H NMR spectra (Figure S13). As the hydrolysis conditions were quite robust, it was necessary to determine the structural integrity of the mixed brush nanoparticles by GPC following hydrolysis. GPC traces before and after hydrolysis for the three brush compositions show no increases in the fraction of single chains, indicating that the crosslinked polymer layers remained intact during hydrolysis (Figure S14, *Supporting Information*). TEM analysis of the three PS/PMAA-CdS samples deposited from THF (Figure S15, *Supporting Information*) revealed the CdS cores to be the same average size (within experimental error) as those present in PS/PMMA-CdS, indicating that the inorganic cores also retained structural integrity during the hydrolysis step.

Comparison of DLS CONTIN size distributions for PS/PMAA-CdS and PS/PMMA-CdS dispersions in THF show a general shift to larger hydrodynamic sizes upon hydrolysis of PMMA chains, with smaller size increases as f_{PS} increases (Figure S16, *Supporting Information*). These shifts in hydrodynamic sizes are attributed to the decrease in solvent quality of THF for hydrophilic PMAA compared to hydrophobic PMMA, with collapse and interparticle aggregation of PMAA chains triggering self-assembly of mixed brush nanoparticles. Based on effective hydrodynamic sizes from DLS measurements at c = ~0.5 mg / mL, the resulting PS/PMAA-CdS assemblies are found to decrease in size as f_{PS} increases, due to the corresponding decrease in the number of collapsed PMAA chains driving self-assembly in THF (Figure 4).

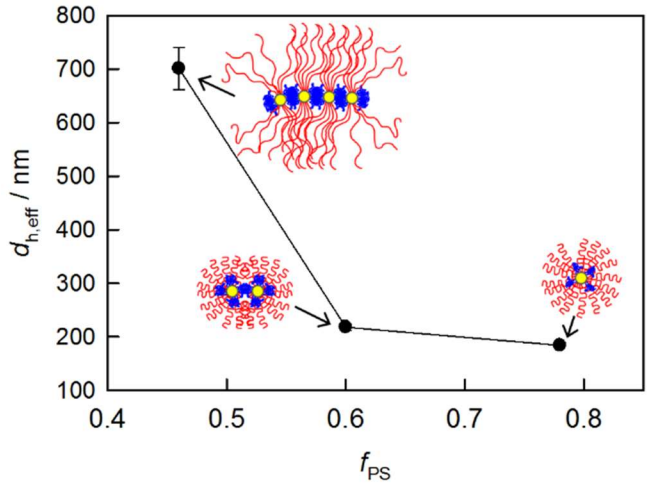

Figure 4. Composition dependence of ABNP self-assembly in an organic solvent. Effective mean hydrodynamic sizes from DLS of PS/PMAA-CdS nanoparticles in THF.

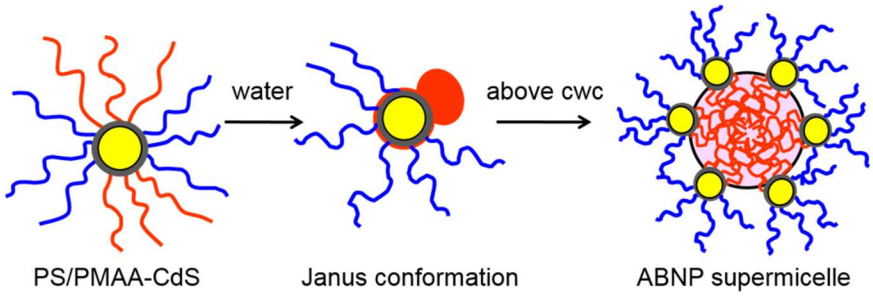

Scheme 3. Conformational rearrangement and self-assembly of PS/PMAA-CdS nanoparticles in THF/water mixtures with increasing water content.

Self-Assembly of PS/PMAA-CdS in THF/Water Mixtures. Dropwise addition of water to PS/PMAA-CdS dispersions in THF leads to an increase in the solubility of PMAA chains and a decrease in the solubility of PS chains. Eventually, PS and PMAA chains segregate to opposite faces of the nanoparticles by wrapping around the core (Scheme 3), enabled by the large radii of gyration of the mixed brushes compared to small the core radii,[22] forming a Janus conformation of broken symmetry. As water addition continues above the critical water content (cwc), the non-centrosymmetric Janus structures undergo amphiphilic self-assembly to form ABNP supermicelles

with PS cores, PMAA coronae, and CdS nanoparticles localized at the interfaces (Scheme 3). Similar to earlier preparations of ABC micellar aggregates in the Eisenberg group,[36] the various ABNP assemblies are transferred to pure water by dialysis prior to characterization. Following dialysis, the resulting aggregates are considered to be kinetically trapped in pure water due to the high T_g of PS.[39] However, their formation in THF/water mixtures just above the cwc occurred under equilibrium conditions, since PS chains will be highly swollen with solvent at low water contents providing dynamic mobility of self-assembling ABNPs. Therefore, unless otherwise noted, the presented TEM images represent snapshots of thermodynamic morphologies in THF/water. Due to the kinetically frozen nature of the PS cores, drying effects have minimal influence on the morphologies imaged by TEM.[33] LSCFM of the self-assembled structures demonstrates fluorescence due to photoemission from constituent CdS nanoparticles (Figure S17, *Supporting Information*).

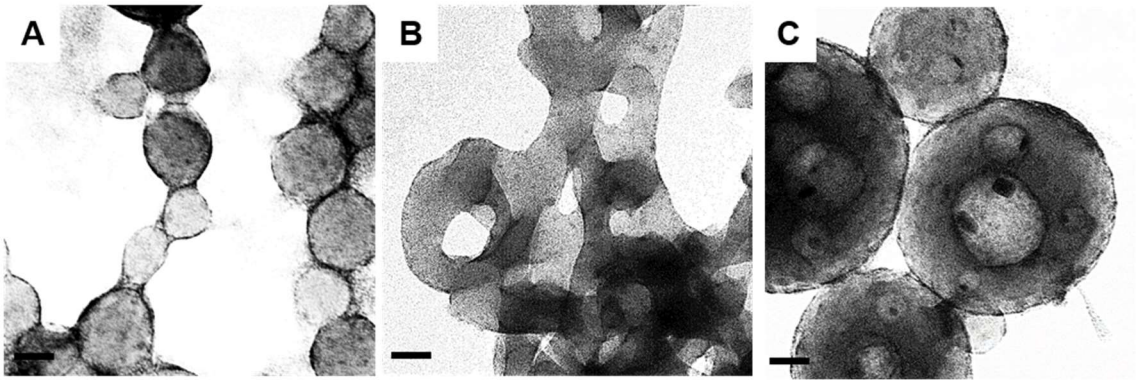

Figure 5. Examples of three main morphology types obtained from self-assembly of PS/PMAA-CdS nanoparticles in THF/water mixtures: A) spheres formed from PS/PMAA-CdS (f_{PS} = 0.5) with no salt addition (R_{NaCl} = 0); B) cylinders formed from PS/PMAA-CdS (f_{PS} = 0.5) with added

salt (R_{NaCl} = 1.5); C) vesicles formed from PS/PMAA-CdS (f_{PS} = 0.6) with added salt (R_{NaCl} = 1.5). For all three preparations, c_0 = 0.5 wt %. All scale bars are 50 nm.

Figure 5 shows examples of the three types of self-assembled morphologies formed from PS/PMAA-CdS in THF/water mixtures by varying brush composition (f_{PS}), initial concentration (c_0) and added salt content (R_{NaCl}). In order of decreasing interfacial curvature, the spheres (Figure 5A), cylinders (Figure 5B), and vesicles (Figure 5C) formed from ABNP self-assembly appear similar to spheres, cylinders, and vesicles formed from self-assembly of PS-*b*-PAA and other ABCs[33] except with dark CdS nanoparticles localized at interfaces. In this section, we will discuss the specific effects of brush composition (f_{PS}), initial nanoparticle concentration (c_0), and salt content (R_{NaCl}) on the self-assembled morphologies. We will then compare the observed trends for ABNPs with literature results for ABC self-assembly, discussing the application of ABC microphase separation principles to nanoscale ABNP building blocks.

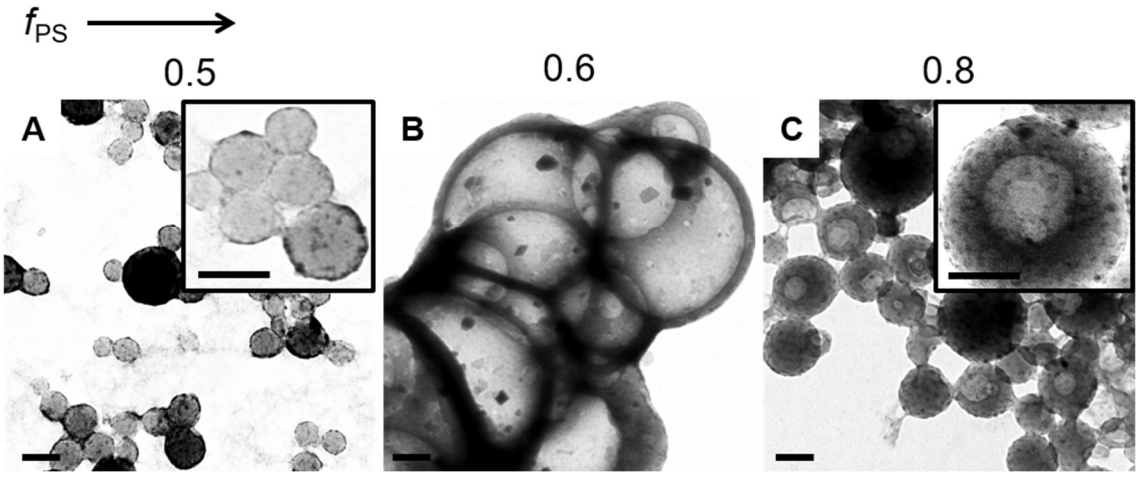

Figure 6. Effect of ABNP brush composition on self-assembly of PS/PMAA-CdS nanoparticles in THF/water mixtures. For all three preparations, c_0 = 0.5 wt % and R_{NaCl} = 0: A) f_{PS} = 0.5; B) f_{PS} = 0.6; C) f_{PS} = 0.8. All scale bars are 100 nm.

Effect of Nanoparticle Brush Composition on Self-Assembled Morphologies. Figure 6 shows the predominant morphologies formed from self-assembly of ABNPs with three different brush compositions at a constant initial nanoparticle concentration of c_0 = 0.50 wt %. Individual CdS nanoparticles are visible as dark dots within each of the nanoparticle assemblies. In order of increasing PS content within the mixed brushes, the predominant self-assembled morphologies are spheres for f_{PS} = 0.5 (Figure 6A), large vesicles for f_{PS} = 0.6 (Figure 6B), and smaller vesicles for f_{PS} = 0.8 (Figure 6C). Spheres are distinguishable from vesicles in the TEM images, being smaller spherical aggregates of lower polydispersity and without one or more discernable low-density compartments. The difference between vesicles and spheres is highlighted in a selected TEM image of the f_{PS} = 0.5 case in which a small number of vesicles co-exist with the predominant spheres (Figure S18, *Supporting Information*). In the f_{PS} = 0.8 case, assignment of the predominant morphology required annealing in THF/water for 2 weeks before quenching and dialysis was carried out, since a mixture of spheres and vesicles were formed without annealing. The persistence of vesicles and disappearance of spheres upon annealing indicated the more thermodynamically stable morphology. For comparison, annealing experiments were also run to confirm the thermodynamic stability of spheres formed from the f_{PS} = 0.5 case (Figure S19, *Supporting Information*).

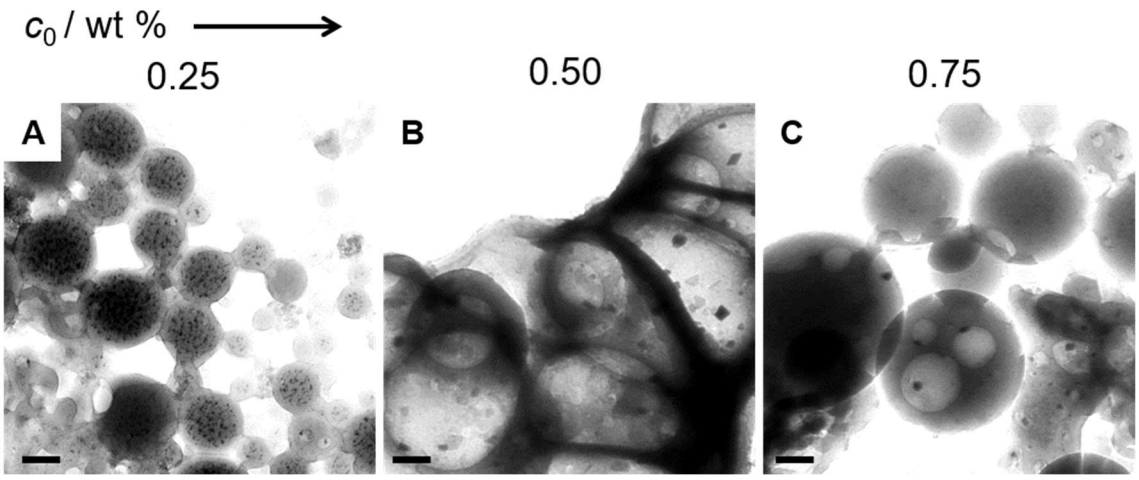

Figure 7. Effect of ABNP initial concentration on self-assembly of PS/PMAA-CdS nanoparticles in THF/water mixtures. For all three preparations, f_{PS} = 0.6 and R_{NaCl} = 0: A) c_0 = 0.25 wt %; B) c_0 = 0.50 wt %; C) c_0 = 0.75 wt %. All scale bars are 100 nm.

TEM data also allowed determination of the degree of PS chain stretching in the cores of the various morphologies, which provides insight into the driving force for observed morphological transitions. The degree of core chain stretching, S_c, is defined as the ratio of the end-to-end distance of PS chains in the core (half the core dimension) to the unperturbed end-to-end distance of the PS blocks (225 repeat units).[33] From the average core diameter of spheres formed in the f_{PS} = 0.5 case (79 nm, *sd* = 22 nm), we determine S_c = 4.0 for this composition, compared to S_c = 1.5 from the average wall thickness of vesicles (29 nm, *sd* = 5 nm) formed in the f_{PS} = 0.6 case. Due to their small lumen sizes, it is difficult to accurately determine wall thicknesses of vesicles in Figure 6C; however, from select particles we estimate the average thickness to be ~20 nm, suggesting an even lower degree of PS stretching (S_c = ~1) in the f_{PS} = 0.8 case. We conclude that as the PS content of constituent ABNPs increases, the resulting self-assembled morphologies transition from a high-curvature PS/PMAA interface (spheres) to a low-curvature interface (vesicles), accompanied by a decrease in the stretching of internal PS blocks.

Effect of Initial Nanoparticle Concentration on Self-Assembled Morphologies. Figure 7 shows the predominant morphologies formed from ABNP self-assembly at three different initial nanoparticle concentrations, c_0, for constant brush composition, f_{PS} = 0.6. The series of images clearly shows that the morphological effect of increasing c_0 for constant f_{PS} is very similar to that of increasing f_{PS} for constant c_0 (Figure 6). Specifically, the morphologies change from spheres (Figure 7A) to large vesicles (Figure 7B) to smaller vesicles (Figure 7C) as c_0 is increased. This suggests that for a constant brush composition, transitions to lower-curvature morphologies (e.g. from spheres to vesicles) become more favourable as the initial ABNP concentration increases.

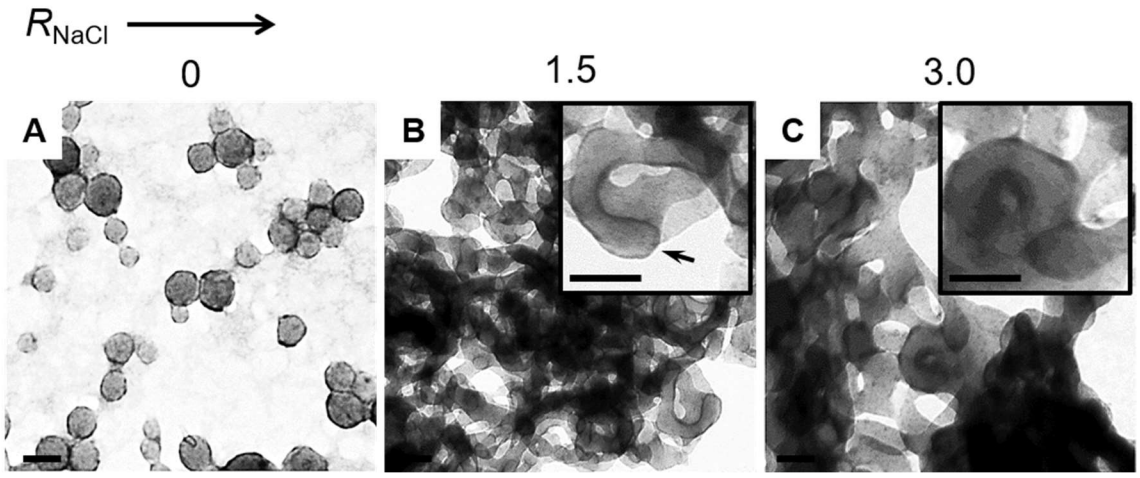

Figure 8. Effect of added salt content on self-assembly of PS/PMAA-CdS nanoparticles in THF/water mixtures. For all three preparations, f_{PS} = 0.5 and c_0 = 0.5 wt %: A) R_{NaCl} = 0; B) R_{NaCl} = 1.5; C) R_{NaCl} = 3.0. All scale bars are 100 nm.

Effect of Added Salt Concentration on Self-Assembled Morphologies. As shown in Figures 6 and 7, ABNP self-assembly gave rise to either high-curvature spheres or low-curvature vesicles under conditions of different f_{PS} and c_0; none of the resulting nine conditions showed a tendency to form intermediate-curvature cylinders. However, we found that cylindrical aggregates could be formed by adding NaCl salt to PS/PMAA-CdS dispersions prior to water addition. Figure 8 shows

the effect of added salt content, R_{NaCl} (ratio of NaCl to methacrylic acid repeat units), on the self-assembled ABNP morphologies at constant f_{PS} = 0.5 and c_0 = 0.50 wt %. As indicated previously, spheres are the predominate morphology without salt addition under these conditions (R_{NaCl} = 0, Figure 8A). However, when salt is added to a ratio of R_{NaCl} = 1.5, the morphology changes to a network of cylinders (Figure 8B). Although the cylinders are highly interconnected, cylinder caps are visible throughout the network as shown in the inset (black arrow). When the added salt content is further increased to R_{NaCl} = 3.0, a similar network of somewhat wider cylinders is obtained (Figure 8C). Compared to the average sphere diameter of 79 nm (*sd* = 22) in the R_{NaCl} = 0 case, the average cylinder widths are determined to be 47 nm (*sd* = 10 nm) and 55 nm (*sd* = 13 nm) for the R_{NaCl} = 1.5 and 3.0 cases, respectively. From these data, we conclude that salt addition drives a morphological transition from high-curvature spheres to medium-curvature cylinders, accompanied by an initial decrease in PS chain stretching from S_c = 4.0 to S_c = 2.4. A further increase in salt content then increases PS stretching within the cylinders, from S_c = 2.4 to S_c = 2.8.

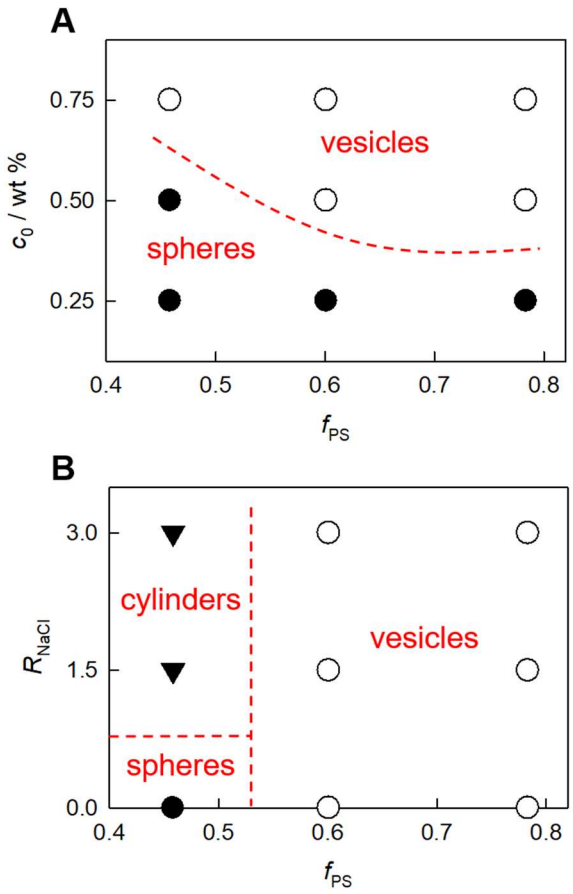

Figure 9. Phase behaviour of PS/PMAA-CdS in THF/water mixtures based on experimentally observed morphologies for variable conditions of: A) c_0 and f_{PS} (constant $R_{NaCl} = 0$) and B) R_{NaCl} and f_{PS} (constant $c_0 = 0.5$ wt %).

Phase Behaviour of ABNPs. The combined morphological effects of brush composition (f_{PS}), initial nanoparticle concentration (c_0), and added salt (R_{NaCl}) are summarized by the phase diagrams in Figure 9, which map the predominant self-assembled ABNP morphologies formed at each of the indicated conditions. Figure 9A maps the c_0-f_{PS} phase behaviour without salt addition ($R_{NaCl} = 0$), with the dashed red line indicating an approximate phase boundary between spheres and vesicles in the diagram. Consistent with the discussion in previous sections, the diagram indicates that the transition from spheres to vesicles becomes favourable as either f_{PS} or c_0 increases. Figure 9B maps the c_0-R_{NaCl} phase behaviour for a constant initial nanoparticle

concentration of c_0 = 0.50 wt %, showing approximate phase boundaries (dashed red lines) between spheres, cylinders, and vesicles. The diagram indicates that vesicles are favoured at the two brush compositions of higher PS content (f_{PS} = 0.6 and 0.8), irrespective of salt addition. On the other hand, at the brush composition of lowest PS content, spheres are favoured without salt addition (R_{NaCl} = 0) while the same ABNPs form cylinders in the presence of salt (R_{NaCl} = 1.5 and 3.0). TEM images corresponding to each of the self-assembly conditions represented in Figure 9, A and B are provided in *Supporting Information* (Figures S20 and S21, respectively).

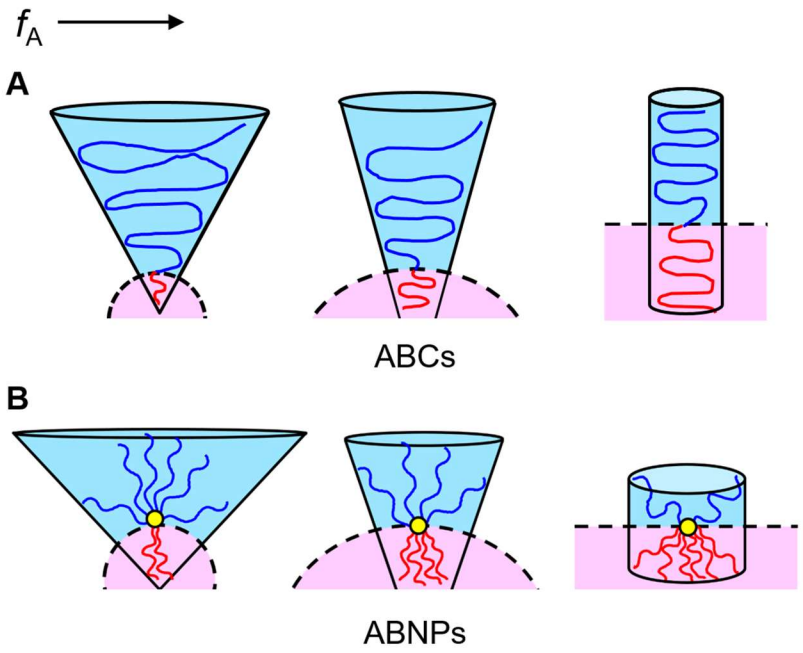

Figure 10. Schematic illustration of core-column models for morphological transitions as the hydrophobic volume fraction f_A increases for A) ABCs and B) ABNPs. In both A and B, red chains represent hydrophobic core-forming sections and blue chains represent hydrophilic corona-forming sections of the respective amphiphiles. Dashed lines represent the core/corona interface.

Comparison of ABC and ABNP Self-Assembly. In their seminal 1996 paper, Eisenberg and coworkers described the thermodynamics of solution self-assembly of ABCs according to the interplay of three Gibbs free energy terms: 1) the interfacial tension between the hydrophobic core and the surrounding aqueous phase, 2) stretching of hydrophobic blocks in the core, and 3) repulsion between hydrophilic blocks in the corona.[36] The interfacial tension term drives close packing of block copolymer junctions at the core-corona interface, decreasing the interfacial energy per chain while also increasing unfavourable core chain stretching and coronal chain repulsion terms. As chain aggregation numbers and packing density increase, interfacial curvature provides an additional degree of freedom for minimizing the total free energy, leading to morphological transitions (e.g. between spheres, cylinders, and vesicles). In this section, we compare trends in ABC morphologies and core dimensions with respect to composition,[35, 36] initial concentration,[38, 39] and salt addition[40, 41] with the current ABNP results. The consistent similarities between these systems suggest analogous thermodynamic terms and microphase separation principles operating for both macromolecular ABC and nanoscale ABNP amphiphiles.

As depicted in Figure 10A, the composition dependence of ABC morphologies can be understood in terms of an increase in the relative importance of core chain stretching compared to coronal chain repulsion as the volume fraction of hydrophobic segments (f_A) increases.[33] As a result, morphological transitions at critical values of f_A lead to lower interfacial curvature which decrease steric interactions and stretching of core-forming blocks. For example, investigation of a series of "crew-cut" PS-*b*-PAA block copolymers with constant PS block length (200 repeat units) in DMF/water mixtures revealed aggregate morphologies changed from spheres (high curvature) to cylinders (intermediate curvature) to vesicles (low curvature) as the PAA block length decreased from 21 to 8 repeat units. Based on core dimensions in the different morphologies, it was

determined that the degree of PS chain stretching decreased as follows: S_c = 1.4 (spheres), 1.3 (cylinders), and 1.0 (vesicles).[36] By comparison, we show that increasing the number fraction of hydrophobic chains (f_{PS}) in ABNP amphiphiles also triggers morphological transitions that decrease interfacial curvature. For example, as summarized in the phase diagram in Figure 9B, increases in f_{PS} lead to transitions from spheres (high curvature) to vesicles (low curvature) in the absence of salt (R_{NaCl} = 0), and from cylinders (intermediate curvature) to vesicles (low curvature) in the presence of salt (R_{NaCl} = 1.5 and 3.0). Similar to the ABC morphological transitions in ref. 36, we also find that lowering curvature of ABNP assemblies leads to corresponding decreases in PS chain stretching (e.g. from spheres with S_c = 4.0 to cylinders with S_c = 2.4; or from spheres to vesicles with S_c = 1.5). Based on these similarities between the effects of f_A on morphologies and core dimensions, we propose that analogous core-column models on different length scales can be applied to ABC (Figure 10A) and ABNP (Figure 10B) self-assembling systems.

In addition to changes in copolymer composition, ABC morphologies are known to depend strongly on the initial polymer concentration (c_0) with increasing c_0 leading to morphologies of decreasing interfacial curvature.[38, 39] This trend has been explained in terms of the known dependence of aggregation numbers on the concentration of small-molecule surfactants:

$$N_{Agg} = 2\left(\frac{c}{cmc}\right)^{1/2}$$

where N_{Agg} is the aggregation number, c is the surfactant concentration, and cmc is the critical micelle concentration in a given solvent system.[44] From the above relation, the aggregation number increases as the amphiphile concentration increases. For ABCs, this leads to an increase in steric interactions between hydrophobic blocks and resulting transitions to lower-curvature interfaces in order to relieve chain stretching in the core. For example, Zhang et al. showed that the block

copolymer PS(410)-*b*-PAA(25) formed spheres, cylinders, and vesicles in DMF/water mixtures when the initial polymer concentrations were 2.0 wt %, 2.6 wt %, and 4.0 wt %, respectively.[38] By comparison, the current case of ABNP self-assembly shows a similar dependence on the initial concentration of amphiphilic building block, with the phase diagram in Figure 9A showing transitions from spheres (high curvature) to vesicles (low curvature) as c_0 increases for all three brush compositions.

Finally, the morphogenic effect of added salt on ABC self-assembly has been well established.[40, 41] Added salt ions screen electrostatic repulsion between charged coronal blocks, increasing the chain packing density which augments steric interactions and stretching of core-forming blocks. As the salt content increases, increased chain stretching leads to an increase in core dimensions until chain stretching reaches a critical extent; then, a morphological transition will occur to lower interfacial curvature thus relieving chain stretching in the core. For example, the self-assembly of PS(410)-*b*-PAA(25) in DMF/water was investigated for different amounts of added NaCl salt, and was found to form spheres with an average diameter of 29 nm without added salt ($R_{NaCl} = 0$).[41] The average size of spheres increased to 33 nm when salt was added to a ratio of $R_{NaCl} = 0.2$, and increased further to 37 nm when the salt ratio was increased to $R_{NaCl} = 0.4$. However, for a salt ratio of $R_{NaCl} = 0.6$, cylinders with average widths of 34 nm were observed; furthermore, vesicles with a wall thickness of ~25 nm were formed when the salt ratio was increased to the range $R_{NaCl} = 1.0$-2.0. Similar to the ABC system, we find that increased salt content increases the core dimensions for a given morphology; specifically, the mean dimension of ABNP cylinders increased from 47 nm to 55 nm when the salt content was increased from $R_{NaCl} = 1.5$ to $R_{NaCl} = 3.0$. Moreover, we find that salt addition can also trigger morphological transitions to lower-curvature interfaces with decreased PS stretching, such as the observed transition from

spheres with $S_c = 4.0$ to cylinders with $S_c = 2.4$ as the salt content increased from $R_{NaCl} = 0$ to $R_{NaCl} = 1.5$, analogous to salt-induced morphological transitions in self-assembling ABCs.

The above correspondence in the behaviour of ABC and ABNP amphiphiles with respect to various self-assembly parameters is consistent with a similar interplay of interfacial tension, core chain stretching and coronal chain repulsion governing morphologies and dimensions in both systems. This suggests that ABC microphase separation principles can be equally applied to controlling the self-organization of ABNPs, despite the disparate length scales of these different types of amphiphilic building blocks. Such scale invariance of self-assembly concepts is understood by considering certain analogous and pertinent structural features of ABCs and ABNPs (following conformational rearrangement of the latter to a Janus state), including spatially distinct and covalently connected hydrophilic and hydrophobic sections, conformational flexibility of hydrophobic sections, and electrostatic repulsion between solubilized hydrophilic sections.

Despite their similarities, a key difference between ABC and ABNP building blocks is highlighted by comparing core dimensions of self-assembled morphologies for the two systems. Namely, comparing the extent of core chain stretching for spheres, cylinders and vesicles within assemblies of ABCs (S_c = 1.4, 1.3, and 1.0, respectively)[36] and ABNPs (S_c = 4.0, 2.4, and 1.5, respectively), we find that the stretching extent of hydrophobic chains of comparable length is 1.5-3× greater within aggregates of the nanoscale amphiphiles. We attribute this difference to the polymer brush structure of Janus-state ABNPs, in which each hydrophobic face consists of multiple PS chains close-packed on the surface of a CdS nanoparticle, leading to internal interchain steric interactions in addition to external steric interactions with neighboring ABNPs at the interface. In contrast, each macromolecular ABC amphiphile consists of a single PS block, significantly reducing steric interactions at the interface compared to self-assembled ABNPs. This

explains the significant reduction in core chain stretching for ABC micelles compared to ABNP supermicelles, and underlines quantitative differences in scale despite qualitative similarities in morphologies and morphological trends. The differences in the specific structure of ABC and ABNP amphiphiles are also significant in that the observed similarities in ABC and ABNP microphase separation principles could not have been assumed *a priori* and thus required direct experimental confirmation as presented in this systematic study of ABNP self-assembly.

Conclusions

The toolbox for the controlled self-assembly of functional inorganic nanoparticles such as quantum dots and gold nanoparticles has been greatly enhanced in recent years by the development of amphiphilic nanoparticles with non-centrosymmetric surface functionality and anisotropic interparticle interactions. Despite experimental work demonstrating complex and variable self-assembly behaviour, and theoretical studies outlining design principles for idealized nanoscale building blocks, a clear set of experimental principles for the controlled self-assembly of amphiphilic nanoparticles akin to those established for amphiphilic block copolymers (ABCs) in the 1990s has been missing from the literature. In their Janus conformational state, amphiphilic brush nanoparticles (ABNPs) resemble nanoscale analogues of ABCs in terms of their distinct but connected hydrophilic and hydrophobic sections, conformational flexibility, and electrostatic interactions. In this study, we produced a well-characterized series of ABNPs, consisting of ~6-nm CdS nanoparticle cores functionalized with mixed polymer brushes of hydrophobic PS and hydrophilic PMAA chains of similar structure (Z = ~110 and σ = ~0.4 chains/nm^2) and variable composition (f_{PS} = 0.5, 0.6, and 0.8). We investigated self-assembly of the ABNPs in THF/water mixtures for different hydrophobic volume fractions (f_A), initial concentrations (c_0) and salt contents (R_{NaCl}), determining the systematic effects of these variables on the resulting self-

assembled morphologies. We showed that amphiphilic self-assembly of ABNPs formed spheres, cylinders, and vesicles analogous to micellar aggregates of ABCs. More importantly, increases in f_A, c_0 and R_{NaCl} were all found to trigger morphological transitions leading to decreased interfacial curvature and concomitant relaxation of core-forming blocks, identical to trends previously established for ABCs, which suggests that ABNPs are governed by a similar balance of interfacial tension, core chain stretching, and coronal chain repulsion. These results bridge the block copolymer and nanoparticle self-assembly paradigms, by showing for the first time that ABC microphase separation principles are scalable to ABNPs. We believe that these guidelines for applying well-established principles for block copolymer self-assembly to more complex ABNPs with interesting optical, electronic or magnetic properties will open up multiple new strategies for designing hierarchical nanomaterials with complex function.

Supporting Information. Experimental details and data on the synthesis and characterization of PS/PMAA-CdS nanoparticles and their assemblies (as described in the main text) are available.

Acknowledgements. We are grateful to the Natural Sciences and Engineering Research Council of Canada, NSERC, for financial support. We acknowledge Dr. Patrick Nahirney and the UVic EM lab (Department of Biology) for the continued use of their TEM.

References

1. Whitesides, G. M.; Grzybowski, B., Self-Assembly at All Scales. *Science* **2002,** *295*, 2418-2421.

2. Jain, P. K.; Huang, X.; El-Sayed, I. H.; El-Sayed, M. A., Noble Metals on the Nanoscale: Optical and Photothermal Properties and some Applications in Imaging, Sensing, Biology, and Medicine. *Acc. Chem. Res.* **2008,** *41*, 1578-1586.

3. Halas, N.; Lal, S.; Chang, W.; Link, S.; Nordlander, P., Plasmons in Strongly Coupled Metallic Nanostructures. *Chem. Rev.* **2011,** *111*, 3913-3961.

4. Xie, J.; Liu, G.; Eden, H. S.; Ai, H.; Chen, X., Surface-Engineered Magnetic Nanoparticle Platforms for Cancer Imaging and Therapy. *Acc. Chem. Res.* **2011,** *44*, 883-892.

5. Murray, C. B.; Norris, D. J.; Bawendi, M. G., Synthesis and Characterization of Nearly Monodisperse CdE (E = Sulfur, Selenium, Tellurium) Semiconductor Nanocrystallites. *J. Am. Chem. Soc.* **1993,** *115*, 8706-8715.

6. Mao, Z.; Xu, H.; Wang, D., Molecular Mimetic Self-Assembly of Colloidal Particles. *Adv. Funct. Mater.* **2010,** *20*, 1053-1074.

7. Nie, Z.; Petukhova, A.; Kumacheva, E., Properties and Emerging Applications of Self-Assembled Structures made from Inorganic Nanoparticles. *Nat. Nanotech.* **2010,** *5*, 15-25.

8. Yang, C.; Li, Q.; Cai, C.; Lin, J., Nanoparticle-Induced Ellipse-to-Vesicle Morphology Transition of Rod–Coil–Rod Triblock Copolymer Aggregates. *Langmuir* **2016,** *32*, 6917-6927.

9. Pan, S.; He, L.; Peng, J.; Qiu, F.; Lin, Z., Chemical-Bonding-Directed Hierarchical Assembly of Nanoribbon-Shaped Nanocomposites of Gold Nanorods and Poly (3-hexylthiophene). *Angew. Chem.* **2016,** *128*, 8828-8832.

10. Choueiri, R. M.; Galati, E.; Klinkova, A.; Thérien-Aubin, H.; Kumacheva, E., Linear Assembly of Patchy and Non-Patchy Nanoparticles. *Faraday Discuss.* **2016,** *191*, 189-204.

11. Hu, J.; Zhou, S.; Sun, Y.; Fang, S.; Wu, L., Fabrication, Properties and Applications of Janus Particles. *Chem. Soc. Rev.* **2012,** *41*, 4356-4378.

12. Walther, A.; Müller, A. H., Janus Particles: Synthesis, Self-Assembly, Physical Properties, and Applications. *Chem. Rev.* **2013,** *113*, 5194-5261.

13. Moffitt, M. G., Self-Assembly of Polymer Brush-Functionalized Inorganic Nanoparticles: from Hairy Balls to Smart Molecular Mimics. *J. Phys. Chem. Lett.* **2013,** *4*, 3654-3666.

14. Yi, C.; Zhang, S.; Webb, K. T.; Nie, Z., Anisotropic Self-Assembly of Hairy Inorganic Nanoparticles. *Acc. Chem. Res.* **2016,** *50*, 12-21.

15. Song, J.; Niu, G.; Chen, X., Amphiphilic-Polymer-Guided Plasmonic Assemblies and Their Biomedical Applications. *Bioconjugate Chem.* **2016,** *28*, 105-114.

16. Nie, Z.; Fava, D.; Kumacheva, E.; Zou, S.; Walker, G. C.; Rubinstein, M., Self-Assembly of Metal-Polymer Analogues of Amphiphilic Triblock Copolymers. *Nat. Mater.* **2007,** *6*, 609-614.

17. Chen, T.; Yang, M.; Wang, X.; Tan, L.; Chen, H., Controlled Assembly of Eccentrically Encapsulated Gold Nanoparticles. *J. Am. Chem. Soc.* **2008,** *130*, 11858-11859.

18. Nikolic, M.; Olsson, C.; Salcher, A.; Kornowski, A.; Rank, A.; Schubert, R.; Fromsdorf, A.; Weller, H.; Forster, S., Micelle and Vesicle Formation of Amphiphilic Nanoparticles. *Angew. Chem. Int. Edit.* **2009,** *48*, 2752-2754.

19. Carbone, L.; Manna, L.; Sönnichsen, C., Self-Assembly of Amphiphilic Nanocrystals. *Angew. Chem. Int. Edit.* **2009,** *48*, 4282-4283.

20. Wang, B.; Li, B.; Dong, B.; Zhao, B.; Li, C. Y., Homo- and Hetero-Particle Clusters Formed by Janus Nanoparticles with Bicompartment Polymer Brushes. *Macromolecules* **2010,** *43*, 9234-9238.

21. Song, J.; Cheng, L.; Liu, A.; Yin, J.; Kuang, M.; Duan, H., Plasmonic Vesicles of Amphiphilic Gold Nanocrystals: Self-Assembly and External-Stimuli-Triggered Destruction. *J. Am. Chem. Soc.* **2011,** *133*, 10760-10763.

22. Zubarev, E.; Xu, J.; Sayyad, A.; Gibson, J., Amphiphilicity-Driven Organization of Nanoparticles into Discrete Assemblies. *J. Am. Chem. Soc.* **2006,** *128*, 15098-15099.

23. Guo, Y.; Harirchian-Saei, S.; Izumi, C. M. S.; Moffitt, M. G., Block Copolymer Mimetic Self-Assemble of Inorganic Nanoparticles. *ACS Nano* **2011,** *5*, 3309-3318.

24. He, J.; Liu, Y.; Babu, T.; Wei, Z.; Nie, Z., Self-Assembly of Inorganic Nanoparticle Vesicles and Tubules Driven by Tethered Linear Block Copolymers. *J. Am. Chem. Soc.* **2012,** *134*, 11342-11345.

25. He, J.; Huang, X.; Li, Y.-C.; Liu, Y.; Babu, T.; Aronova, M. A.; Wang, S.; Lu, Z.; Chen, X.; Nie, Z., Self-Assembly of Amphiphilic Plasmonic Micelle-Like Nanoparticles in Selective Solvents. *J. Am. Chem. Soc.* **2013,** *135*, 7974 - 7984.

26. Liu, Y.; Li, Y.; He, J.; Duelge, K. J.; Lu, Z.; Nie, Z., Entropy-Driven Pattern Formation of Hybrid Vesicular Assemblies Made from Molecular and Nanoparticle Amphiphiles. *J. Am. Chem. Soc.* **2014,** *136*, 2602-2610.

27. Li, W.; Thanneeru, S.; Kanyo, I.; Liu, B.; He, J., Amphiphilic Hybrid Nano Building Blocks with Surfactant-Mimicking Structures. *ACS Macro Lett.* **2015,** *4*, 736-740.

28. Kuttner, C.; Chanana, M.; Karg, M.; Fery, A., *Macromolecular Decoration of Nanoparticles for Guiding Self-Assembly in 2D and 3D*. Wiley-VCH, 2016.

29. Zhang, Z.; Horsch, M.; Lamm, M.; Glotzer, S., Tethered Nano Building Blocks: Toward a Conceptual Framework for Nanoparticle Self-Assembly. *Nano Lett.* **2003,** *3*, 1341-1346.

30. Zhang, Z.; Glotzer, S., Self-Assembly of Patchy Particles. *Nano Lett.* **2004,** *4*, 1407-1413.

31. Davis, J. R.; Panagiotopoulos, A. Z., Monte Carol Simulations of Amphiphilic Nanoparticle Self-Assembly. *J. Chem. Phys.* **2008,** *129*, 194706.

32. Li, Z.-W.; Lu, Z.-Y.; Sun, Z.-Y.; An, L.-J., Model, Self-Assembly Structures, and Phase Diagram of Soft Janus Particles. *Soft Matter* **2012,** *8*, 6693-6697.

33. Mai, Y.; Eisenberg, A., Self-Assembly of Block Copolymers. *Chem. Soc. Rev.* **2012,** *41*, 5969-5985.

34. Zhang, L.; Eisenberg, A., Formation of Crew-Cut Aggregates of Various Morphologies from Amphiphilic Block Copolymers in Solution. *Polym. Advan. Technol.* **1998,** *9*, 677-699.

35. Zhang, L.; Eisenberg, A., Multiple Morphologies of "Crew-Cut" Aggregates of Polystyrene-*b*-poly(acrylic acid) Block Copolymers. *Science* **1995,** *268*, 1728-1731.

36. Zhang, L.; Eisenberg, A., Multiple Morphologies and Characteristics of "Crew-Cut" Micelle-like Aggregates of Polystyrene-*b*-poly(acrylic acid) Diblock Copolymers in Aqueous Solutions. *J. Am. Chem. Soc.* **1996,** *118*, 3168-3181.

37. Yu, Y.; Zhang, L.; Eisenberg, A., Morphogenic Effect of Solvent on Crew-Cut Aggregates of Amphiphilic Diblock Copolymers. *Macromolecules* **1998,** *31*, 1144-1154.

38. Zhang, L.; Eisenberg, A. In *Structures of "Crew-Cut" Aggregates of Polystyrene-b-poly (acrylic acid) Diblock Copolymers*, Macromol. Symp. 1997 Wiley Online Library; pp 221-232.

39. Zhang, L.; Eisenberg, A., Thermodynamic vs Kinetic Aspects in the Formation and Morphological Transitions of Crew-Cut Aggregates Produced by Self-Assembly of Polystyrene-*b*-poly(acrylic acid) Block Copolymers in Dilute Solution. *Macromolecules* **1999,** *32*, 2239-2249.

40. Zhang, L.; Yu, K.; Eisenberg, A., Ion-Induced Morphological Changes in "Crew-Cut" Aggregates of Amphiphilic Block Copolymers. *Science* **1996,** *272*, 1777-1779.

41. Zhang, L. E., A., Morphogenic Effect of Added Ions on Crew-Cut Aggregates of Polystyrene-*b*-poly(acrylic acid) Block Copolymers in Solutions. *Macromolecules* **1996,** *29*, 8805-8815.

42. Guo, Y.; Moffitt, M. G., Semiconductor Quantum Dots with Environmentally Responsive Mixed Polystyrene/Poly(methyl methacrylate) Brush Layers. *Macromolecules* **2007,** *40*, 5868-5878.

43. Guo, Y.; Moffitt, M., "Smart" Self-Assembled Quantum Dots Regulate and Stabilize Structure in Phase-Separated Polymer Blends. *Chem. Mater.* **2007,** *19*, 6581-6587.

44. Israelachvili, J., *Intermolecular and Surface Forces, 2nd Ed.*; Academic Press Ltd. San Diego, 1992.